Applied Physics Letters

The control of thermal conductivity through coherent and incoherent phonon scattering in 2-dimensional phononic crystals by incorporating elements of self-similarity

Cite as: Appl. Phys. Lett. **115**, 213903 (2019); https://doi.org/10.1063/1.5123311
Submitted: 06 August 2019 . Accepted: 07 November 2019 . Published Online: 19 November 2019

D. Banerjee, O. Vizuete, H. Ranjan, S. Pal, and Z.-B. Zhang

Applied Physics Letters ARTICLE scitation.org/journal/apl

The control of thermal conductivity through coherent and incoherent phonon scattering in 2-dimensional phononic crystals by incorporating elements of self-similarity

Cite as: Appl. Phys. Lett. **115**, 213903 (2019); doi: 10.1063/1.5123311
Submitted: 6 August 2019 · Accepted: 7 November 2019 ·
Published Online: 19 November 2019

D. Banerjee,[1,a)] O. Vizuete,[2] H. Ranjan,[3] S. Pal,[1] and Z.-B. Zhang[2,a)]

AFFILIATIONS

[1]CSIR-Central Electronics Engineering Research Institute, Pilani 333031, Rajasthan, India
[2]Solid State Electronics, Department of Engineering Sciences, Ångströmlaboratoriet, Uppsala University, Uppsala 75121, Sweden
[3]Indian Institute of Engineering Science and Technology, Shibpur, Howrah 711103, West Bengal, India

[a)]Electronic addresses: debashree@ceeri.res.in; zhibin.zhang@angstrom.uu.se

ABSTRACT

In this letter, we report the theoretical study on phonon transport in monocrystalline silicon thin-films having unfilled or metal-filled circular holes (i.e., phononic crystals, PnCs) and show that the thermal conductivity, κ, at 1 K can be maximally reduced by using a multiscale structure, which allows us control over the porosity of the structure. The circular scatterers are placed in the square (SQ) and hexagonal (HX) pattern with a fixed 100 nm interhole spacing, and the pit diameter is varied between 10 and 90 nm. Each of the corresponding silicon PnCs shows reduced κ compared to the unpatterned film. The SQ-PnC having tungsten-filled pits shows the greatest reduction in κ when we consider only the effects of coherent scattering. Furthermore, we have computed κ for the PnC where the unit cell, of 100 nm and 500 nm sizes, comprises the Sierpinski gasket (SG) with circular holes of different diameters (depending on the fractal order) in the same cell. It is observed that the κ for the 2nd (100 nm cell) and 3rd order (500 nm cell) SG-PnC is comparable to the SQ- and HX-PnC with a pit diameter of 90 nm. When we add the effect of the diffuse boundary scattering in κ, there is a lowering in κ compared to that when only the coherent effects are considered. The additional κ-reduction due to boundary scattering for the SQ-PnC and HX-PnC (both with 90 nm diam) as well as the 2nd and 3rd order SG-PnCs is 47%, 40%, 80%, and 60%, respectively.

A two-dimensional (2D) phononic crystal (PnC) is a periodic arrangement of elastic-wave reflection sites in a planar host material. The elastic-wave packets are the low frequency phonons that comprise a major contributor in transporting thermal energy from point to point in a solid crystalline material. Each scattering site constitutes a finite discontinuity in the host material due to its complete removal or replacement with materials having a different mass density and/or a different crystalline phase with different elastic properties. The wave scattering results in a modification of the allowed frequencies of the phonons in the different directions of the artificial phononic crystal, which in turn alters the thermal conductivity, κ, of the host material. The use of two-dimensional PnC for the suppression of κ has been increasing not only for engineered thermoelectric materials,[1–6] commonly referred to as "holey silicon,"[1] but also for such applications where the sensitivity of chemical and temperature sensors needs to be boosted,[7,8] for low temperature thermal isolation for various sub-Kelvin applications in physics and astronomy,[9,10] in thermal devices,[11] and for heat guiding.[12] Irrespective of the targeted application area, there are two possible reasonings put forward for the observed reduction in the thermal conductivity. The interference of the phonon waves reflected from the periodically situated gaps specifically introduced in the material leads to a redistribution of the allowed phonon frequencies. This in turn changes the phonon group velocity and density of states. As a consequence, the κ is modified. The other reason often attributed to the κ-reduction is that the random scattering of the phonons from the rough surfaces reduces the phonon mean free path. However, the temperature range where the two different mechanisms are dominant has been progressively worked-out with the reports that the acoustic phonon dispersion relation can be modified by the elastic wave interference, which is a

coherent process, to temperatures of 10 K.[13] For higher temperatures, the effect of the periodic hole arrangement is not different from that of the random arrangement of the holes.[13,14] The reason for this is that the order of the surface roughness, being comparable to the thermal phonon wavelengths at the particular temperature, results in noncoherent diffuse scattering from the roughness. Recently, it has been theorized that the Akhiezer mechanism is responsible for the lack of coherent effects in thin film PnCs in the temperature range of 130–300 K.[15] Quasiballistic transport was, however, reported in corrugated nanowires even at room temperature.[16] To be able to maximize the suppression in thermal conductivity, it is attractive to be able to include both the coherent and incoherent scattering deterministically by the regular placement of the holes of a PnC. The arbitrary nature of the surface roughness leads to uncontrolled phonon scattering and is challenging to design in conformity with specifications. One of the ways to achieve control is to use the self-repeating patterns of a fractal,[17] which not only yield coherent scattering but can also maximize the incoherent boundary scattering as the multiscale structure offers a larger scattering surface.

This work presents the systematic study of the square, hexagonal, and self-repeating lattice structures for their ability to suppress the thermal conductivity compared to the unpatterned single crystal silicon film at a temperature of 1 K. In principle, the simulation model may be used for temperatures up to 10 K, where it was experimentally confirmed that the coherent effects are observable.[13]

The finite-element method has been used for modeling the low frequency phonons in the two-dimensional thin film of monocrystalline (mc-) silicon where they are modeled by the propagation of elastic waves in linear homogeneous solid materials. Artificial holes or gaps are distributed in a periodic fashion in the thin film in either a square (SQ) or hexagonal (HX) pattern. Since thin films of silicon show greatly suppressed κ due to enhanced interface scattering,[18] it is a practical choice to use thin films instead of bulk materials. The dispersion relation is obtained for the unit cell of the SQ and HX lattices along the boundaries of the first irreducible Brillouin zone (IBZ), and the high symmetry points are denoted in the usual $\Gamma - X - M$ notation, as shown in Figs. 1(a) and 1(b) for the HX and SQ lattices, respectively. The phonon wavelength is much larger than the mesh element dimensions, and hence the error arising from the meshing is neglected. The Floquet boundary conditions are implemented at the unit cell edges, while the circular edge of the holes allows free vibrations. The effect of changing the hole diameter or "neck" size, both indicated in Fig. 1(b) for the SQ lattice, is investigated when the separation between the pits is fixed at 100 nm. A third structure where the unit cell consists of multidimensional holes as shown in Fig. 1(c) is considered. The unit structure of Fig. 1(c), which is a Sierpinski gasket[19] (SG), shows the second order repetition of the circular pit. The symmetry of the SG structure is assumed to be similar to the SQ lattice, and the unit cell is tiled in the x- and y-directions in the same way, keeping the primary circular pits fixed 100 nm or 500 nm apart (two unit-cell sizes are considered).

The following elasticity matrix parameters have been used in the simulations, i.e., $C_{11} = 165.6$ GPa, $C_{12} = 63.9$ GPa, and $C_{44} = 79.5$ GPa.[20] The temperature-dependent variation of the elastic constants of silicon[21] is small for the temperature range of interest and hence not considered for the purpose of the study. It was further verified that such a variation does not lead to a significant effect on the degree of

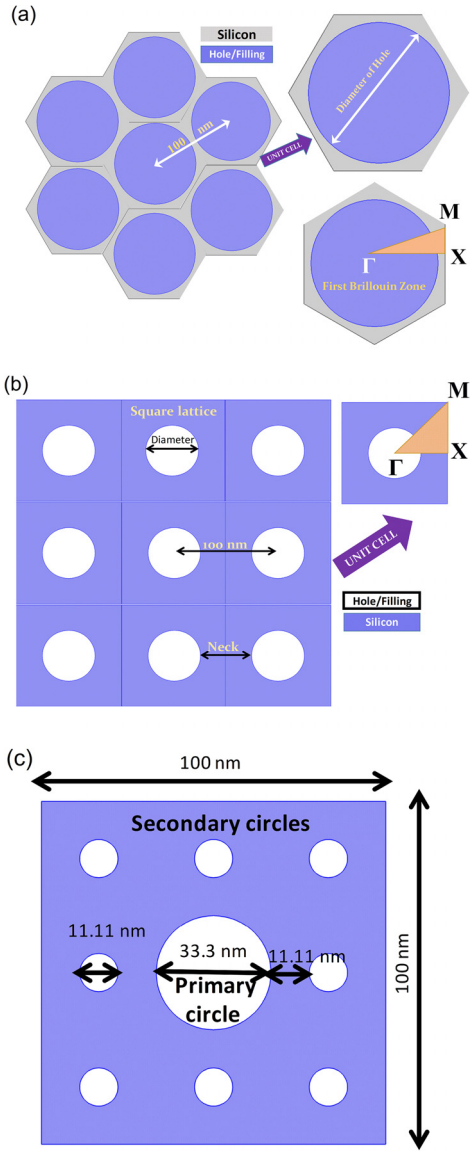

FIG. 1. (a) A schematic of the hexagonal lattice, the hexagonal unit cell, and the irreducible Brillouin zone (IBZ). The high symmetry points are denoted by $\Gamma - X - M$ and (b) a two-dimensional square lattice schematic along with its unit cell and IBZ; (c) a second order self-repeating structure using the circular structure. The circle diameters are scaled as $D_n = a/3^n$, where n is the order of the structure and a is the size of the unit cell.

suppression of the thermal conductivity. Considering that filling the holes with large mass difference materials will lead to enhanced scattering of the phonons,[18] the pits are likewise filled with iron and tungsten and compared to the multiscale structure. The mass densities of mc-Si, tungsten, and iron considered in the model are 2330 kg/m^3, 19 350 kg/m^3, and 7870 kg/m^3,[22] respectively. It is seen from the mass density differences between mc-Si and the metals that the scattering due to tungsten filling is expected to be the highest, while the iron filling may not lead to a remarkable degree of such scattering. The elastic matrix of W is

$C_{11} = 520$ GPa, $C_{12} = 200$ GPa, and $C_{44} = 160$ GPa, while that of Fe is $C_{11} = 237$ GPa, $C_{12} = 141$ GPa, and $C_{44} = 116$ GPa.[22] The temperature range of operation of the phononic crystals is limited to 1 K since the dominant phonon frequency at this temperature is ~33.2 GHz calculated from $f_{2D} = \frac{1.594 k_B T}{h}$,[23] and using reasonable computational resources, phonon frequency up to ~250 GHz (~7.5 f_{2D}) was obtained by evaluating the first hundred eigenmodes of the infinite lattice using 31 data points on the Brillouin zone boundaries.

The thermal conductivity, κ, is modeled by the Holland Callaway model[24] in the frequency domain by the expression, $\kappa = \frac{1}{6\pi^2}\int_0^{\omega_0} C_{ph} v_g^2 \tau D \, d\omega$, where C_{ph} is the heat capacity at a frequency ω, v_g the phonon group velocity at frequency ω, $\tau = \frac{L}{v_g}$ the scattering time including only the boundary scattering since it is assumed that all other mechanisms are frozen out at 1 K, L the minimum feature size or the neck size, and D the density of states at the frequency ω and summed over all dispersion branches. The thermal conductivity of the PnC (κ) is normalized with the thermal conductivity of the unpatterned membrane (κ_0) to represent the degree of suppression obtained due to the PnC patterning. The simulator had been validated against the existing literature[25] to ascertain the accuracy of our simulation as compared to the more resource intensive model, and comparable trends are observed (details in the supplementary material).

At first, we consider the effect of only the coherent phonon scattering to determine the relative effectiveness of the three structures to impede the flow of heat at 1 K. In the interim when we ignore the boundary scattering, we find from Fig. 2(a) that for the unfilled SQ lattice (black square), as the pit diameter increases, κ is suppressed to a greater degree than the suppression predicted by the Maxwell-Eucken model (violet asterisk). The Maxwell-Eucken model, $(1-\varphi)/(1+(2/3)\varphi)$, with φ being the porosity, predicts that κ can be lowered simply due to the removal of matter when the pits are introduced in the unpatterned material. It is observed that there is no significant advantage of using iron filling (red circle) in the circular holes, and the PnC performance is similar to that of unfilled holes. When the holes are lined with heavy tungsten, there is a remarkable increase in suppression of κ till hole diameters of 50 nm. For hole diameters from 50 nm to 70 nm, the change in the degree of κ-suppression as a function of the hole diameter flattens. One can see that the W-filled SQ-PnC offers the largest degree of κ-suppression over the entire size range, although the κ/κ_0-value reaches a valley and increasing the hole size further, beyond 50 nm, does not offer any additional advantages. It is observed from Fig. 2(b) that the hexagonal lattice displays similar performance to the square lattice for both W-filled and unfilled holes. The observed suppression in thermal conductivity can be understood by examining the dispersion relations of the PnCs. As shown in Fig. 2(c), a magnified frequency vs reduced wave-vector dispersion diagram of the SQ-PnC having a pit diameter of 80 nm, both partial ($\Gamma - X$, $X - M$) and complete frequency gaps ($\Gamma - X - M - \Gamma$) are present as marked in shadow. In addition, the SQ-PnC has a greater number of complete gaps for 80 nm and 90 nm diameters of the holes, as shown in Fig. 2(d), and therefore has lower κ than the HX-PnC [Fig. 2(b)]. For the entire range of the circular hole sizes, the HX-PnC has manifold partial frequency gaps along the $M - \Gamma$ direction, while the SQ-PnC has none. Nevertheless, this does not yield a lowered κ-value for the HX-PnC, confirming that the frequency gaps in the backward direction of the wave-vector do not favorably alter κ. The number of partial frequency gaps along the $\Gamma - X$ and $X - M$ directions in Fig. 2(d) is alike for the different hole diameters of the HX- and SQ-unfilled PnCs and for the frequency range simulated here. Thus, we see a similar degree of κ-suppression in Fig. 2(b) for the two types of PnCs with unfilled holes.

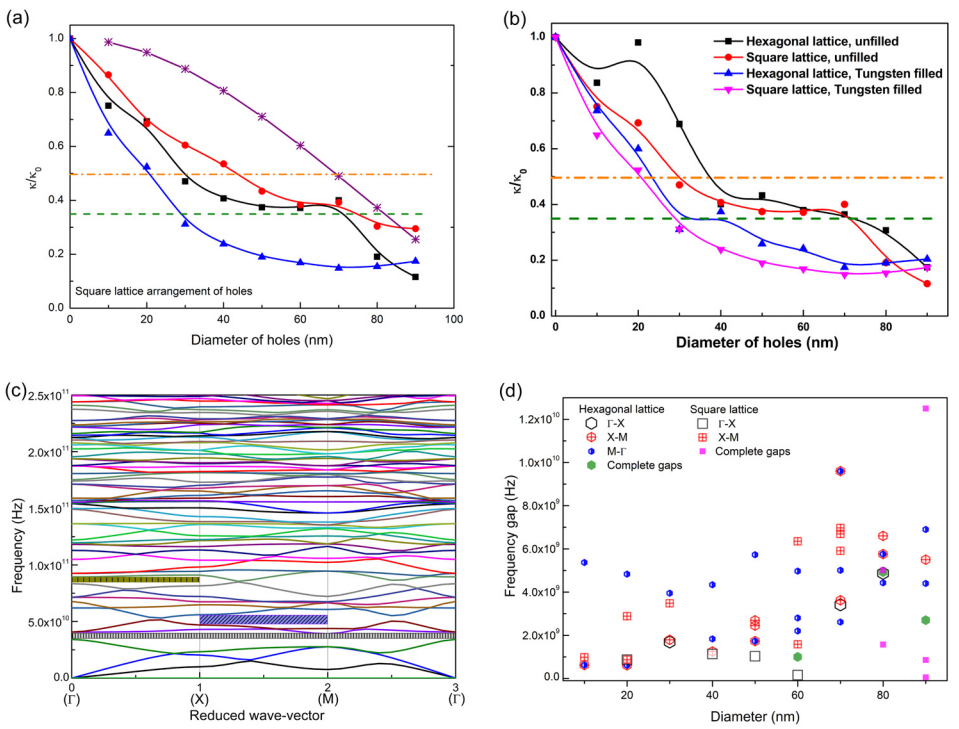

FIG. 2. (a) The normalized thermal conductivity at 1 K as a function of the diameter for unfilled (black square), iron-filled (red circle), and tungsten-filled (blue triangle) circular inclusions in monocrystalline Si (100 nm thick) arranged in a square lattice ($a = 100$ nm) and the Maxwell-Eucken model predictions (purple asterisk) for the same structure. The data for the unit cells of the first order (orange dashed-dotted line) and second order (olive dashed line) Sierpinski gasket are shown in the same figure and (b) the comparison of the thermal conductivity suppression in the case of the tungsten-filled square (magenta inverted triangle) and hexagonal lattice (legends, same as that of the square lattice) for different diameters of the circular lattice elements; (c) a portion of the frequency vs reduced wave-vector dispersion diagram for a square lattice having holes of diameter 80 nm and (d) the frequency bandgap of the dispersion diagram of the phononic crystal for unfilled square and hexagonal lattice as a function of the hole diameter.

The interhole separation of 100 nm is used for the highest-level circular inclusions in the hierarchy of the multiscale structure (SG-PnC), which is thus the unit cell size, to enable direct comparison with the conventional 2D lattice of the PnCs. The first order SG structure has only one circle at the center and has performance identical to the corresponding SQ lattice structure. The porosity factor, $\varphi\left(=\frac{\text{area of the circular hole}}{\text{area of the unit cell}}\right)$, of the artificial crystals is compared for the conventional 2D crystal lattice of SQ and HX arrangement with the multiscale structures in Fig. 3(a). The intersection of the arrows with the porosity curves for the SQ and HX lattices shows the corresponding dimensions required to achieve similar porosity to the SG structures. The second order fractal, whose schematic is shown in Fig. 1(c), with holes of two diameters in a single unit cell, 33 nm (primary circle) and 11 nm (secondary circles), exhibits a higher porosity than what a SQ or HX lattice can achieve if they contain individual holes of diameters equal to the secondary or primary circles alone. Thus, using multiple holes of different diameters within a single unit cell, the multiscale structure can achieve lower κ as can be perceived by using the Maxwell-Eucken model. When we consider solely the coherent phonon scattering due to the incorporated circular pits, the second order SG-PnC offers κ lowering similar to the unfilled SQ and HX lattice of hole diameters ~70 nm. Using the SG-PnC instead of the SQ- or HX-PnC with a larger hole diameter is thus advantageous since the mechanical strength of the SQ/HX-PnC is less due to large portions of material removed [hence highly porous, Fig. 3(a)]. On the other hand, more surface area is available for incoherent phonon scattering in the SG-PnC than in the SQ-PnC for similar levels of porosity. Therefore, the boundary scattering effect is included and the κ reduction is re-evaluated as shown in Fig. 3(b). The κ/κ_0-values are plotted when the coherent effects are accounted for exclusively (the dark shadow bar-graph) and when the incoherent scattering is additionally reckoned (of the light shadow bar-graph). In the latter case, we note that even for the SQ and HX structure, the improvement is considerably more than earlier ~47% and 40%, respectively, for the PnC with 90 nm diameter holes. The second order SG structure with the additional incoherent effects, having a separation of 100 nm between the primary holes, produces a drastic blockage of thermal flow (better by 80%) when compared to the occasion where only the coherent effect is considered. It is further noted in Fig. 3(b) that for a larger structure with a 500 nm hole-to-hole separation of the primary first order holes, the third order structure gives an even greater hindrance to thermal conduction due to the large surface scattering and has performance similar to the highly porous structure of 90 nm hole diameter SQ and HX lattice structures (further details in the supplementary material). An anomalous behavior is observed in the case of the first order SG-PnC with the incoherent effects leading to higher values of κ/κ_0 compared to the exclusively coherent case. Similar behavior is observed for certain values of diameter for SQ and HX PnC and has been explained in the supplementary material.

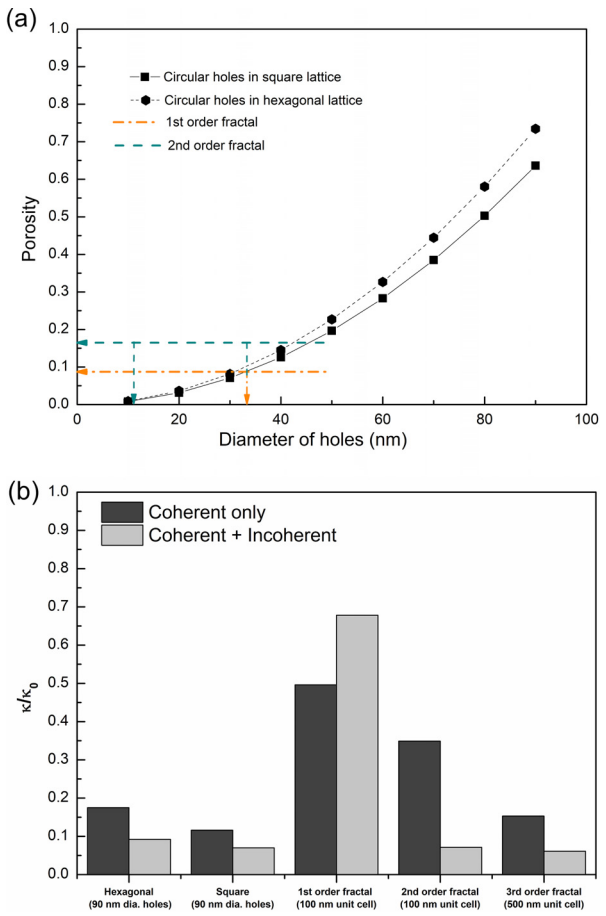

FIG. 3. (a) The geometrical porosity factor variation with the dimension of the holes for square and hexagonal lattices. The porosity of the structure incorporating the 1st and 2nd order fractals for $a = 100$ nm is marked by dashed-dotted and dashed arrows, respectively, and (b) shows the thermal conductivity in the square and hexagonal lattice at 1 K temperature when considering only the coherent scattering at the inclusions vs when the phonon scattering at the boundary surfaces is included for these geometries. It is observed that the impact of the phase noncorrelated boundary scattering is most prominent in the geometries that incorporate the self-repeating structures.

In conclusion, this letter presents an efficient FEM-based simulation method to study the comparative performance of the different nanoengineered structures in thin-film monocrystalline silicon. The simulation evaluates the modification to the phonon propagation, which ultimately leads to a decrement of the phonon thermal conductivity as compared to a pristine film of the same material. The model operating temperature of 1 K unambiguously preserves the coherent wave effects. We find that the multiscale hierarchical structure of the repeating arrangement of the circular holes in the mc-Si film enables strong suppression of the phononic thermal conductivity and even offers advantages of relaxed fabrication tolerance by using larger geometrical parameters. The significant advantage of using a self-replicating structure in making the phononic crystal is that we can algorithmically control the magnitude of surface scattering of phonons while still maintaining the coherent scattering phenomena.

See the supplementary material for validation of the present study against the existing literature and explanation of the anomalous increase in the thermal conductivity for a certain structure of the PnC.

This work was supported by the Department of Science and Technology, New Delhi, India (Grant No. DST/INSPIRE/04/2016/000903) and the Swedish Research Council (Grant No. 621–2014-5596).

REFERENCES

[1]J. Tang, H.-T. Wang, D. H. Lee, M. Fardy, Z. Huo, T. P. Russell, and P. Yang, Nano Lett. **10**, 4279 (2010).
[2]N. K. Ravichandran and A. J. Minnich, Phys. Rev. B **89**, 205432 (2014).
[3]G. Romano and J. C. Grossman, Appl. Phys. Lett. **105**, 033116 (2014).
[4]J. Nakagawa, Y. Kage, T. Hori, J. Shiomi, and M. Nomura, Appl. Phys. Lett. **107**, 023104 (2015).
[5]J. Lee, J. Lim, and P. Yang, Nano Lett. **15**, 3273 (2015); M. Nomura, J. Nakagawa, K. Sawano, J. Maire, and S. Volz, Appl. Phys. Lett. **109**, 173104 (2016).
[6]S. Hu, J. Chen, N. Yang, and B. Li, Carbon **116**, 139 (2017).
[7]R. Lucklum and J. Li, Meas. Sci. Technol. **20**, 124014 (2009).
[8]R. Lucklum, Procedia Eng. **87**, 40 (2014).
[9]J. Wei, D. Olaya, B. S. Karasik, S. V. Pereverzev, A. V. Sergeev, and M. E. Gershenson, Nat. Nanotechnol. **3**, 496 (2008).
[10]A. V. Feshchenko, O.-P. Saira, and J. P. Pekola, Sci. Rep. **7**, 41728 (2017).
[11]Y. Feng and X. Liang, J. Heat Transfer **139**, 052402 (2017).
[12]R. Anufriev, A. Ramiere, J. Maire, and M. Nomura, Nat. Commun. **8**, 15505 (2017).
[13]J. Marie, R. Anufriev, R. Yanagisawa, A. Ramiere, S. Volz, and M. Nomura, Sci. Adv. **3**, e1700027 (2017).
[14]M. R. Wagner, B. Graczykowski, J. S. Reparaz, A. E. Sachat, M. Sledzinska, F. Alzina, and C. M. S. Torres, Nano Lett. **16**, 5661 (2016).
[15]Y. Liao, T. Shiga, M. Kashiwagi, and J. Shiomi, Phys. Rev. B **98**, 134307 (2018).
[16]R. Anufriev, S. Gluchko, S. Volz, and M. Nomura, ACS Nano **12**, 11928 (2018).
[17]B. Mandelbrot, *The Fractal Geometry of Nature* (Times Books, 1982).
[18]W. Liu and M. Asheghi, Appl. Phys. Lett. **84**, 3819 (2004).
[19]N. Gao, J. H. Wu, and L. Jing, Mod. Phys. Lett. B **29**, 1550134 (2015).
[20]M. A. Hopcroft, W. D. Nix, and T. W. Kenny, J. Microelectromech. Syst. **19**, 229 (2010).
[21]T. Goto, H. Y-Kaneta, Y. Saito, Y. Nemoto, K. Sato, K. Kakimoto, and S. Nakamura, J. Phys. Soc. Jpn. **75**, 044602 (2006).
[22]The mass densities of mc-Si. Tungsten and Iron and elastic matrices of Tungsten and Iron are the default values supplied by the COMSOL Multiphysics.
[23]N. Zen, T. A. Puurtinen, T. J. Isotalo, S. Chaudhuri, and I. J. Maasilta, Nat. Commun. **5**, 3435 (2014).
[24]I. El-kady, R. H. O. Iii, P. E. Hopkins, Z. C. Leseman, D. F. Goettler, B. Kim, C. M. Reinke, and M. F. Su, Progress Report No. SAND2012-0127, Sandia National Laboratories, CA, 2012.
[25]R. Anufriev and M. Nomura, Phys. Rev. B **95**, 155432 (2017).